NIH Public Access
Author Manuscript
Mol Cancer Res. Author manuscript; available in PMC 2011 October 1.

Published in final edited form as:
Mol Cancer Res. 2010 October ; 8(10): 1319–1327. doi:10.1158/1541-7786.MCR-09-0551.

Rapid Extravasation and Establishment of Breast Cancer Micrometastases in the Liver Microenvironment

Michelle D. Martin[1,*], **Gert-Jan Kremers**[2], **Kurt W. Short**[2], **Jonathan V. Rocheleau**[3], **Lei Xu**[4], **David W. Piston**[2], **Lynn M. Matrisian**[1], and **D. Lee Gorden**[1,5]

[1]Department of Cancer Biology, Vanderbilt University

[2]Department of Molecular Physiology and Biophysics, Vanderbilt University

[3]Institute of Biomaterials and Biomedical Engineering, University of Toronto

[4]Department of Biostatistics, Vanderbilt University

[5]Department of Surgery, Vanderbilt University

Abstract

To examine the interplay between tumor cells and the microenvironment during early breast cancer metastasis, we developed a technique for *ex vivo* imaging of murine tissue explants using two-photon microscopy. Cancer cells in the liver and the lung were compared by imaging both organs at specific time points after the injection of the same polyoma middle T-initiated murine mammary tumor cell line. Extravasation was greatly reduced in the lung compared to the liver, with 56% of tumor cells in the liver having extravasated by 24 hours, while only 22% of tumor cells in the lung had done so. In the liver, imaged cells continually transitioned from an intravascular location to an extravascular site, while in the lung extravasation rates slowed after 6 hours. Within the liver microenvironment, the average size of the imaged micrometastatic lesions increased 4-fold between days 5 and 12. Histologic analysis of these lesions determined that by day 12 the micrometastases were heterogenous, consisting of both tumor cells and von Willebrand Factor-positive endothelial cells. Further analysis with iv-administered lectin indicated that vessels within the micrometastatic tumor foci were patent by day 12. These data present the use of two-photon microscopy to directly compare extravasation times in metastatic sites using the same tumor cell line, and highlight the differences in early events and metastatic patterns between two important secondary sites of breast cancer progression with implications for future therapy.

Keywords

breast cancer; metastasis; two-photon microscopy; liver; imaging

Introduction

The liver is one of the most common solid organ sites of metastasis for breast cancer. In spite of this, the liver microenvironment remains understudied even though patients with liver metastases comprise a poor prognosis group with median survival rates of less than 6 months and reduced response to systemic therapy [1-3]. The site of tumor metastasis is influenced by

Copyright © 2010 American Association for Cancer Research

[*]To whom correspondence should be addressed Vanderbilt University, 771 Preston Research Building, 2220 Pierce Avenue, Nashville TN 37212 Telephone: 615-343-3422 Fax: 615-936-2911 michelle.d.martin@vanderbilt.edu .

NIH-PA Author Manuscript
NIH-PA Author Manuscript
NIH-PA Author Manuscript

NIH-PA Author Manuscript

NIH-PA Author Manuscript

NIH-PA Author Manuscript

both the primary tumor cell and the distant microenvironment into which it spreads, and therefore it is important to better understand the role of the liver microenvironment in early breast cancer metastasis. [4,5].

One of the earliest events in metastasis is the extravasation of tumor cells from the vasculature into the surrounding stroma of the metastatic site. Previous work from different groups has shown that the time to extravasation of tumor cells can differ in distinct microenvironments. The work of Morris et al. determined that greater than 95% of the malignant melanoma cells injected into the liver extravasated [6]. However, Muschel and colleagues have observed attachment of both HT1080 fibrosarcoma cells and 4T1 mammary carcinoma cells to the endothelium and intravascular growth in the lung vasculature [7,8]. It is not clear if these discrepancies are the result of differences in technical approach, in tumor cell type, and/or organ microenvironments.

The development of two-photon excitation microscopy has made it possible to examine tumor cells inside the intact organ microenvironment in which they reside based upon the ability of the laser to penetrate deeper into tissue and provide richer detail than standard one photon confocal microscopy techniques [9,10]. This is especially beneficial for highly autofluorescent tissues such as the liver. This technique has been previously used to visualize tumor cells in sites including the mammary fat pad and the lung [7,10,11]. Past experiments using two-photon microscopy to investigate early metastatic tumor cell behavior has yielded varying results depending on both the type of tumor cells used and the site at which they are imaged [8,11, 12]. Therefore, for our study, we utilize the same breast cancer cell line in all of our imaging studies in order to directly compare the effect of two distinct microenvironments on early tumor cell extravasation and establishment.

We developed a technique for *ex vivo* two-photon imaging of the liver and lung microenvironments in a murine model in an effort to better understand tumor/stromal interactions at these important secondary sites. Stromal cells were found to incorporate in micrometastatic colonies and patent vasculature was visualized as early as twelve days following tumor cell injection in the liver. A clearer understanding of the earliest events in metastatic tumor establishment has therapeutic implications for cancer patients that currently do not respond well to systemic therapy.

Results

Development of Two-Photon Ex Vivo Liver Imaging Method

The R221A clonal cell line was isolated from a mammary tumor in the MMTV-PyVT mouse on the FVB/N background and engineered to stably express green fluorescent protein (GFP) as previously described [13,14]. These cells can be injected into a FVB/N syngenic host that is fully immunocompetent, allowing studies that consider the role of the immune system in tumor phenotype. For the establishment of metastases in an experimental model of liver metastasis, 1×10^6 R221A-GFP cells were injected into the spleen of an anesthetized female mouse and reached the liver via the hepatic portal circulation to form multi-focal metastatic disease in the liver. These cells have been previously shown to form reliable, reproducible liver metastases in our hands (unpublished data), and our laboratory has prior experience using the splenic injection model to induce liver metastases [15]. For the establishment of lung metastases, 1×10^6 R221A-GFP cells were injected into the lateral tail vein of an anesthetized female mouse as previously described [14]. A complex of biotinylated tomato lectin and streptavadin coated Qdot585 was injected into either the spleen and heart (for liver imaging) or the heart alone (for lung imaging) to bind and label the vasculature (Figure 1A, 1D). The complex uniformly labeled the vasculature of both organs, except when the presence of tumor cells in the vessels significantly obstructed the binding of the vascular label. The mice were

NIH-PA Author Manuscript

NIH-PA Author Manuscript

NIH-PA Author Manuscript

then perfused with phosphate buffered saline (PBS) under gravity pressure so as not to introduce artificially elevated pressures into the pulmonary or systemic circulations, in order to remove blood from the liver or lung that would interfere with the imaging of green fluorescent protein. The excised intact organs were then placed onto a microscopy dish and imaged immediately. Multiple z-stacks ranging from 20-100 μm thick were recorded at random areas containing tumor cells. We were able to successfully separate the signals from the GFP expressing tumor cells and the Qdot- labeled vasculature, resulting in three dimensional datasets clearly denoting the relationship of tumor cells to the liver (Figure 1B, 1C) and lung vasculature (Figure 1E, 1F).

Influence of Metastastatic Site on Time to Extravasation

To investigate whether differences in the liver and lung microenvironments impacted the timing of extravasation of the breast tumor cells, liver and lung experimental metastasis models were compared using the same breast cancer cell line. Liver and lung explants were imaged at 2, 6, 12, and 24 hours after tumor cell injection to compare the percentage of tumor cells that had extravasated in each metastatic site. To determine the location of tumor cells in relation to the vasculature, we utilized both 3-dimensional reconstructions as well as viewing the orthogonal planes from the imaged stacks (Figure 1 B, C, E, F, supplemental movies 1B, 1C, 1E, 1F). At 24 hours post tumor cell injection the majority of tumor cells in the liver had extravasated (56%). In contrast, at this time only a minority of the tumor cells in the lung had extravasated (22%) (Table 1). These results are similar to those reported by Muschel and colleagues who observed minimal extravasation of HT1080 and 4T1 cells in the lung at 24 hours [7, 8].

By directly comparing the time course of tumor cell extravasation in the liver to that in the lung, we determined that extravasation proceeds throughout a 24 hour window in the liver (Figure 2A), while the small amount of extravasation seen in the lung occurs mostly within 6 hours following tumor cell injection (Figure 2B). Image analysis revealed that that the time point at which the majority of breast cancer cells move from an intravascular to an extravascular site in our liver metastasis model occurred between 12 and 24 hours post-injection (Figure 2A, Table 1). Between these time points the majority of imaged tumor cells became localized in the extravascular space, while in contrast, at 24 hours the majority of breast cancer cells remained within the vasculature of the lung (Figure 2B, Table 1). By 24 hours, the estimated probability of a cell being located in the extravascular space was significantly different in the liver relative to the lung ($p= 0.0001$).

Determination of Stromal Cells Present in Micrometastatic Lesions in Liver

Since the majority of tumor cells in the liver had extravasated by 24 hours post tumor cell injection, we next sought to determine features of how these cells established themselves in the liver microenvironment. All imaged lesions at 5 and 12 days post tumor cell injection had extravasated and consisted principally of GFP-labeled tumor cells, but also appeared to contain a proportion of unlabeled cells of host origin (Figure 3A, arrowheads, 3E). Immunofluorescence was performed on 5 μm sections of 5 and 12 day livers that had previously been imaged with two-photon microscopy to determine the lineage of these cells. Our first goal was to determine if these host cells were bone-marrow derived, as it is known that macrophages, neutrophils, and mast cells are very important to early tumor establishment and growth [16-18]. Antibodies directed against CD45 were used to broadly identify bone marrow-derived cells, and antibodies directed against GFP were used to identify the tumor cells (Figure 3B, 3F). It was noted that although some CD45-positive cells were within a few of the early lesions (arrowhead, Figure 3F), these CD-45-positive cells were not abundant enough to account for all of the unlabeled cells within the foci. Based upon these findings we concluded that CD45

NIH-PA Author Manuscript

NIH-PA Author Manuscript

NIH-PA Author Manuscript

positive cells recruited from the host bone marrow did not constitute the majority of unlabeled cells within the lesions.

We next wanted to determine if the majority of unlabeled cells in the early micrometastatic lesions were endothelial cells contributing to the establishment of early vascular networks. Antibodies directed against von Willebrand Factor (vWF) and GFP were used to label endothelial cells and tumor cells, respectively (Figure 3C, figure 3G). Staining for vWF was also used to assess both mature and neo-vasculature within the 5 day and 12 day tumor foci. Tumor foci stained for vWF indicated significantly more vWF-positive vasculature in the day 12 lesions (arrowheads, Figure 3G) than the day 5 lesions (Figure 3C, 3D). To determine if the vessels were patent, the livers of tumor-bearing mice were perfused with a complex of biotinylated lectin and streptavadin Alexa fluor 568 before sacrifice. Five day tumor foci did not appear to contain any patent vessels, although in some instances they were in close proximity to patent vessels also positive for vWF (data not shown). By 12 days after tumor cell injection, the micrometastatic tumor foci contained vessels with a functional lumen (Figure 3H, inset arrow).

Analysis of Progression of Micrometastatic Lesions in the Liver

We next sought to track the sizes of the micrometastatic lesions at 5 and 12 days following tumor cell injection. To accomplish this, two-photon imaging was performed on *ex vivo* explants of livers at 5 days and 12 days post-injection (Figure 3A, 3E). Z-stacks in random areas of the liver that contained tumor cells were analyzed and volumetric analysis was used to determine the distribution of tumor volumes. At 5 days, the majority of lesions imaged had not surpassed 2×10^5 μm^3 (Figure 4A), with the average volume of the lesions being 9×10^4 μm^3. By 12 days, the distribution of tumor volumes had changed; a number of lesions were larger than 1×10^6 μm^3 (Figure 4B) and the average size of the lesions increased 4-fold to 3.6×10^5 μm^3. Interestingly, however, at 12 days the majority of micrometastatic lesions remained small, i.e., a volume of 2×10^5 μm^3 or less. While the majority of lesions at day 5 consisted of a few cells at most, by day 12 those lesions that had a larger volume appeared to consist of a small colony of cells. This data suggested that there were two subsets of lesions: a majority that remained the same size between days 5 and 12, and consisted of a few cells at most, and a subset that had the capacity to form a small micrometastatic lesion in the liver microenvironment.

Discussion

Two-photon microscopy allows for the examination of the interaction of tumor cells with their microenvironment at the very earliest steps in metastasis. We have adapted two-photon microscopy for the *ex vivo* examination of tumor cells in the liver utilizing a whole organ preparation that is useful for studying single cells and micrometastases in situ. We utilized this system to examine the influence of different microenvironments on tumor cell extravasation. Results demonstrated that the same tumor cell type extravasated more in the liver than in the lung. Although data analysis in the lung microenvironment was more challenging than the liver microenvironment due to the structure of the lung, we extensively analyzed numerous images to accurately determine the position of the tumor cells relative to the blood vessels. Multiple mice and multiple views of each mouse were utilized to ensure that enough data was gathered and analyzed to enable us to make well-informed determinations of the locations of the tumor cells that could then be compared using statistical analyses. These analyses provided strong evidence supporting our conclusions that extravasation times differ between the liver and the lung, as the p-value for testing whether metastatic tumor cells in the liver or lung had achieved extravasation by 24 hours was 0.0001. Given this finding, the probability of observing the differences of a cell being extravascular at 24 hours between liver and lung by chance is less

NIH-PA Author Manuscript

NIH-PA Author Manuscript

NIH-PA Author Manuscript

than 0.0001. We also show that the critical time for tumor cells to extravasate in the liver was between 12 and 24 hours after tumor cell injection, and by 5 days after tumor cell injection, all cells that we imaged had extravasated. Early metastases in the liver are heterogeneous colonies, consisting of GFP-positive tumor cells, the occasional CD45-positive bone marrow-derived cell, and vWF-positive endothelial cells. At 12 days post tumor cell injection, some lesions contained patent vasculature. Volumetric analysis of these early lesions at 5 and 12 days post tumor cell injection determined that at both time points the majority of lesions that were imaged had a volume smaller than 2×10^5 μm^3. By 12 days post-injection the distribution had changed, showing a broad range of tumor volumes. However, even the lesions with the largest volume at day 12 (1.3×10^6 μm^3) did not reach the size typically associated with lesions that have reached a size limit requiring them to undergo angiogenesis to sustain their growth (1-2 mm in diameter). These finding are important as they add to the understanding of the earliest features in the progression of breast cancer metastases in the liver.

It is well known that the site of metastasis is influenced by interactions between the tumor cells and the microenvironment at the metastatic site [19,20]. Our studies are unique in that they are the first to examine the behavior of the same breast cancer cell line in two clinically relevant metastatic sites. In addition, our studies utilize two-photon microscopy, which enables us to examine the location and growth of tumor cells deeper in the intact organ than previous studies that utilized confocal microscopy. This is particularly important for autofluorescent tissues such as the liver. These results could lead to a better understanding of early tumor/stromal interactions in the liver microenvironment and point towards the utility of using this microscopy technique for the study of early metastasis in different organ microenvironments.

Prior work that involved the study of early metastasis to the lung and liver environments has yielded differing results concerning cellular location after arrival in the metastatic site. In the lung microenvironment, work from the Muschel group has shown convincingly that both 4T1 mammary carcinoma cells and HT1080 fibrosarcoma cells injected intravenously tended to remain within the vasculature and formed intravascular colonies [7-8]. Our studies indicate that there is minimal extravasation of MMTV-polyoma middle-T derived mammary carcinoma cells in the lung. In the liver microenvironment, tumor cell arrest in the organ and the rate of extravasation from the microvasculature appear to depend in part upon the model system and the tumor cell line used for the studies. In two studies using intravital fluorescence microscopy with mammary and melanoma cell lines, it was found that the initial arrest of the cancer cells in the sinusoids of the liver was due to size restriction [6,21]. We noted that in some instances our results showed that some of the tumor cells in the vessels prevented the binding of the vascular label, in agreement with the results above. However, work by Haier et al. in which intravital microscopy was performed on the surface of rat livers after injection of colon carcinoma cells, determined that the tumor cells adhered to sinusoidal capillaries whose diameter was larger than that of the tumor cells [22]. Our results suggested this was also occurring in our model, as we were able to visualize tumor cells bound to vessels with clear vascular labeling distal to the tumor cells. Our studies to determine the time course for extravasation in the liver microenvironment determined that tumor cell extravasation occurs continually, with the majority of the breast tumor cells in the liver having extravasated at 24 hours after injection. The difference in extravasation in these two organs could simply be a consequence of the differences in the architecture of the vasculature of the liver and lung. The liver contains a fenestrated endothelium which controls microvascular exchange that is not seen in the lung, and could impact the ability of cells to transmigrate from the vessels to the stroma of the liver [23]. Alternatively, our observed results may denote differences in interactions between the tumor cells and the host cells of the respective microenvironments. Elucidating these mechanisms and the differences in liver and lung extravasation is the subject of ongoing work.

NIH-PA Author Manuscript

NIH-PA Author Manuscript

NIH-PA Author Manuscript

Our studies also determined that the majority of early metastatic foci formed in the liver consisted of only a few cells even at 12 days after tumor cell injection (Figure 4B). There was also a subset of foci that showed a broad distribution in size. Recent work by Qian et al. [24] has shown that stromal cues, at least in the lung microenvironment, are provided by CD11b +Gr1- macrophages that enhance metastatic extravasation, survival, and outgrowth. While we did not test for specific markers of macrophage subsets in our studies, we did note that there were CD45-positive bone marrow derived cells within a small subset of the micrometastatic lesions 12 days following tumor cell injection (Figure 3F). Though few in number, these accompanying CD45-positive cells could contribute to the outgrowth of these lesions by providing a permissive microenvironment for the tumor cells. Importantly, a subset of lesions imaged at day 12 appeared to contain functional vessels (Figure 3G, 3H). Additionally, the vascular staining index was significantly higher in the 12 day lesions as compared to the 5 day lesions although the size of the lesions was smaller than that typically associated with angiogenesis [25]. We noted that, in general, as tumor size increased, the vascular staining index increased. This would suggest that those lesions that could utilize an existent patent blood supply early in their development were able to thrive in the liver microenvironment, while the majority of lesions that did not utilize a blood supply remained dormant in the liver. However, there were some outliers that either were large and did not contain many vessels, or were small and contained a significant amount of vessels (data not shown). These results demonstrated some of the spatial heterogeneity of the vasculature network that has been previously described in tumors [26-28].

In summary, our studies developed a method for the analysis of the location and outgrowth of breast cancer cells in both the liver and lung microenvironments using two-photon microscopy, and determined that these cells extravasated more in the liver compared to the lung microenvironment. Our findings present evidence that the location of the tumor cells once they reach the metastatic site is dependent on a variety of both tumor and microenvironmental factors. Of the tumor cells that extravasated into the liver parenchyma, only a subset were able to develop into micrometastatic lesions by 12 days after tumor cell injection, and these lesions contained patent vasculature. This suggests that the acquisition of a functional vasculature is a rare event, but may be essential for early metastatic tumor establishment in the liver microenvironment, as proposed by Folkman and others [29]. These observations may impact therapy for breast cancer patients in the future. While a proportion of patients in the clinic present with well defined metastases, others have no evidence of metastatic lesions but have a high risk of developing metastases from existing lesions that are below the limits of detection of current imaging modalities. Improved knowledge of the patterns of micrometastatic establishment in specific microenvironments would provide the possibility of targeting therapy in the future to interfere with specific early steps of metastasis.

Materials and Methods

Animal models

All studies were conducted following review and approval by the Vanderbilt Institutional Animal Care and Use Committee. FVB/N mice were purchased from the Jackson Laboratory. R221A-GFP tumor cells previously generated by the laboratory [13] were used for all assays. We verified the R221A-GFP cell line by morphological and growth rate analysis as per ATCC guidelines to assure they had not become altered from the parental cells isolated from a PyVT mouse in our laboratory prior to starting any of the experiments in this manuscript. The cells were maintained in selection media (DMEM (Invitrogen, Carlsbad, CA) containing 10% FCS (Atlanta Biologicals, Norcross, GA) and 10 μg/ml puromycin (Sigma, St. Louis, MO) plus gentamycin (Invitrogen). For the experimental model of liver metastasis, 6-8 week old female mice were anesthetized using 2% isoflurane (Baxter, Deerfield, IL), then 1×10^6 R221A-GFP

NIH-PA Author Manuscript

NIH-PA Author Manuscript

NIH-PA Author Manuscript

cells in a total volume of 100μl phosphate buffered saline (PBS) were injected using a 27.5 gauge into the spleen as previously described [15]. Hemostasis of the spleen was assured with electrocautery, and the spleen was placed back into the abdominal cavity which was closed in appropriate layers using 5-0 prolene suture. For the experimental model of lung metastasis, 1×10^6 R221A-GFP cells in a total volume of 100μl PBS was injected into the tail vein of 6-8 week female mice as previously described [14].

Preparation of vascular labels

To make the lectin-Qdot complex, a mixture containing a final concentration of 2μM biotinylated tomato lectin (Vector Labs, Burlingame, CA), 0.1μM Q-dot-585- streptavidin conjugate (Invitrogen) and 40mM sodium borate, pH 8.3 (Sigma-Aldrich, St. Louis, MO) was incubated for 2 hours at room temperature. It was next filtered through a Microcon Ultracell YM-100 column (Millipore, Bedford, MA) and resuspended in 100μl of PBS (pH 7.4) per mouse for injection at the time of imaging. For the vasculature label that utilized Alexa Fluor 568 (Invitrogen), a mixture containing a final concentration of 9.6μM biotinylated tomato lectin (Vector Labs) and 9.4μM Alexa Fluor 568-streptavadin conjugate (Invitrogen) was incubated for 20 minutes at room temperature before injection into mice at the time of imaging. This alternative labeling approach was required due to the loss of Qdot fluorescence following fixation.

Preparation of livers and lungs for ex-vivo imaging

At the specified time for two-photon microscopy imaging, mice were anesthesized using Ketamine and Xylazine (Fort Dodge Animal Health, Fort Dodge, Iowa) at a dose of 90 mg/kg Ketamine, 5 mg/kg Xylazine by IP injection and placed on mechanical ventilation at a rate of 60 breaths/minute through a surgical tracheostomy. For liver imaging, the abdomen was prepped in sterile fashion and the spleen was isolated by opening up the abdomen through the previous incision used to inject the tumor cells into the spleen. The tomato lectin-Qdot vascular label was injected into the spleen and allowed to circulate throughout the body for 6 minutes. Next, the suprahepatic and infrahepatic venacaval portions, as well as the abdominal aorta, were isolated and cut with scissors to provide outflow without increasing pressure within the liver. Mice were perfused using gravity pressure to rid the liver of blood and hemoglobin that interferes with the imaging of GFP. Perfusion under gravity resulted in a pressure significantly lower than systemic pressure in the animal. After the effluent had cleared, the liver was resected en-bloc, placed in a glass bottom dish (MatTek Corp., Ashland, MA) and immediately imaged using two-photon microscopy. All organ explants were completely imaged within 45 minutes of removal from the animal to minimize any confounding effects due to cellular and tissue breakdown occurring in the resected organ. For imaging of lung, a similar preparation was done with a few alterations. For labeling the vasculature of the lungs, the lectin/Qdot complex was injected into the right ventricle of the still beating heart. The lungs were then perfused with PBS through both the left and right ventricles, and resected in the inflated state by tying off the trachea.

For the analysis of vascular patency, mice were anesthesized using 2% isoflurane (Baxter, Deerfield, IL), and the abdomen was opened. The lectin/Alexa Fluor 568 complex was injected into the spleen and allowed to circulate throughout the body for 6 minutes. The chest was then rapidly opened and the vasculature was perfused with 3% paraformaldehyde in PBS (pH 7.4) through an 18 gauge needle. Perfusion was done through both the spleen and the left ventricle of the heart. The liver was then removed, immersed in fixative for 4 hours at 4°C, then processed and sectioned for immunofluorescence.

NIH-PA Author Manuscript

NIH-PA Author Manuscript

NIH-PA Author Manuscript

Histology and immunohistochemistry

Liver tissues were placed into 3% paraformaldehyde (EMD Biosciences, San Diego, CA) for 24 hours then moved to a 20% sucrose solution for 48 hours. The tissues were then embedded in Tissue Freezing Medium (Triangle Biomedical Sciences, Durham, NC) and stored at −20° C for sectioning. For immunohistochemistry, 5μm sections of liver were assessed for expression of GFP using a goat anti-GFP antibody (Abcam, Cambridge, MA), for CD45 using an anti-mouse antibody (Serotech, Raleigh, NC), and for von Willebrand factor using a rabbit polyclonal anti-vWF antibody (Dako, Carpinteria, CA. Alexa Fluor secondary antibodies were used in all staining (Invitrogen). For negative controls of CD45 and vWF, mouse IgG and rabbit IgG were used, respectively (Sigma, St. Louis, MO). Staining for cell nuclei was done with Hoechst #33258 (Sigma). Widefield fluorescent microscopy was done on an Axioplan 2 Zeiss automated upright microscope (Carl Zeiss, Inc., Thorwood, NY). Imaging was done using the PlanNEOFLUAR 20X (NA 0.5) and the PlanApochromat 40X (NA 1.0) objectives. Images were detected using an Orca ER camera (Hammamatsu, Bridgewater, NJ). Staining for vWF was used to calculate the Vascular Staining Index. This measurement consisted of the average intensity of staining multiplied by the percent of tumor foci area that is positively stained for the marker. Therefore, this measurement is a method of analyzing the amount of blood vessels per area of tumor foci. Images were acquired and analyzed using Metamorph software version 7.5 (Molecular Devices, Downingtown, PA).

Two-photon microscopy

Two-photon imaging was performed using a LSM510 laser scanning microscope with a Fluar 20×0.75 NA objective (Carl Zeiss, Inc., Thorwood, NY). Two-photon excitation was provided by a Coherent Chameleon Ti:Saphire laser tuned to 880 nm (Coherent Inc., Santa Clara, CA). Green (GFP) and red (Qdot-585) fluorescence was separated by a DCLP540 dichroic mirror and detected simultaneously by two non-descanned detectors. Scanning was done at 512×512 pixels (154 μm×154 μm) and z-stacks (20-100 μm thick) were recorded by taking images at a 1μm interval. These settings resulted in a voxel volume of 0.09 μm^3 (*i.e.* 0.3 μm× 0.3 μm× 1 μm).

Volumetric analysis of tumors

Average tumor volume at day 5 and day 12 were determined by segmenting the tumor tissue in each z-stack based on the GFP fluorescence. Z-stacks were median filtered and a threshold was applied to select for GFP fluorescence. The segmentation was refined by a series of opening and closing operations. Tumor volumes were converted from voxels to μm^3 by multiplying with the voxel volume (0.09 μm^3).

Image segmentation was done using MATLAB 6.1 (The MathWorks, Natick, MA) and the image processing library DIPlib (Pattern Recognition Group, TU Delft, the Netherlands, (http://www.ph.tn.tudelft.nl/DIPlib/).

Ex-vivo data analysis and image processing

Ex-vivo image data were analyzed by visual inspection. Tumor cells were divided into 2 subclasses, intravascular or extravascular, based upon their location relative to the vasculature. In order to determine the location of a cell, a variety of images were analyzed, including 3D representations of the image stack and orthogonal images of the stack. The criteria that determined if a cell was intravascular was the presence of red vascular label that completely surrounded the cell in both the orthogonal and 3D representations. For the determination of a cell being extravascular, the cell either had no red surrounding it in the images, or was incompletely surrounded by red vascular label. Cells were called undetermined if their localization could not be accurately resolved.

NIH-PA Author Manuscript

NIH-PA Author Manuscript

NIH-PA Author Manuscript

Ex-vivo image data presented in figures 1A and 1D represents maximum projections of 15 μm thick subsets selected from the z-stacks. Before generating the maximum projections the subsets were median filtered and the fluorescence signals were contrast enhanced to facilitate visualization. Image processing was done using the Zeiss LSM510 imaging software.

Statistical Analyses

To model the percentage of extravascular cells at specific time points we fit a logistic regression model using both the liver and the lung data. Tumor environment (liver or lung), time and their interaction are included as factors. The differences of percentage of extravascular cells imaged between the liver and the lung microenvironments at each time point can be tested by looking at the interaction terms. The estimated probability of extravasation and its 95% confidence intervals at each time point are shown in Table 1. More tumor cells in the liver extravasate over time than in the lung. The differences between the two become statistically significant at 24 hours. For the vascular staining index data as measured by staining for vonWillebrand's factor, we first checked the normality assumption using normal qq plots (results not shown). The distribution of the vascular staining index at day 5 and day 12 is displayed using a box plot in figure 3D. Both the qq plot and the Box plots indicated that the distribution of the index was highly skewed and not likely to be normal. Therefore the non-parametric Wilcoxon Rank-sum test was used to compare the median of the vascular staining index between the two time points. All analyses were performed and the graph in Figure 3D were generated using R, an open source free software for statistical computing and graphics (http://www.r-project.org/). The bar graphs in Figure 4 were generated using Igor Pro 5.0 software (Wavemetrix, Portland, OR), and the line graphs in Figure 2 were generated using GraphPad Prism 5 (GraphPad Software, Inc., La Jolla, CA).

Supplementary Material

Refer to Web version on PubMed Central for supplementary material.

Acknowledgments

Experiments were performed in part through the use of the VUMC Cell Imaging Shared Resource (supported by NIH grants CA68485, DK20593, DK58404, HD15052, DK59637, and EY08126). The authors wish to acknowledge the generous help of the laboratory of Ruth Muschel M.D., Ph.D., in early discussions and training related to multiphoton microscopy. In addition, the authors acknowledge Alessandro Ustione who was involved in the development of the imaging technique.

This work was supported by R03DK078711, K08DK70708-01 (to DLG), R01CA084360 (to LMM), P20GM72048 (to DWP), and R25CA092043 (appointment to MDM) from the NIH.

References

1. Pentheroudakis G, Fountzilas G, Bafaloukos D, et al. Metastatic breast cancer with liver metastases: a registry analysis of clinicopathologic, management and outcome characteristics of 500 women. Breast Cancer Res Treat 2006;97:237–244. [PubMed: 16322882]
2. Lubrano J, Roman H, Tarrab S, Resch B, Marpeau L, Scotte M. Liver resection for breast cancer metastasis: does it improve survival? Surg Today 2008;38:293–299. [PubMed: 18368316]
3. Pouillart P, Jouvet M, Palangie T, et al. Hepatic metastases of breast cancer. Analysis of the parameters which influence the response to chemotherapy. Ann Gastroenterol Hepatol (Paris) 1985;21:87–90. [PubMed: 4004142]
4. Paget S. The distribution of secondary growths in cancer of the breast. Lancet 1889;1:571–573.
5. Price JE, Naito S, Fidler IJ. Growth in an organ microenvironment as a selective process in metastasis. Clinical and Experimetnal Metastasis 1988;6:91–102.

NIH-PA Author Manuscript

NIH-PA Author Manuscript

NIH-PA Author Manuscript

6. Morris VL, MacDonald IC, Koop S, Schmidt EE, Chambers AF, Groom AC. Early interactions of cancer cells with the microvasculature in mouse liver and muscle during hematogenous metastasis: videomicroscopic analysis. Clin Exp Metastasis 1993;11:377–390. [PubMed: 8375113]
7. Wong CW, Song C, Grimes MM, et al. Intravascular location of breast cancer cells after spontaneous metastasis to the lung. Am J Pathol 2002;161:749–753. [PubMed: 12213701]
8. Al-Mehdi AB, Tozawa K, Fisher AB, Shientag L, Lee A, Muschel RJ. Intravascular origin of metastasis from the proliferation of endothelium-attached tumor cells: a new model for metastasis. Nat Med 2000;6:100–102. [PubMed: 10613833]
9. Piston DW. The coming of age of two-photon excitation imaging for intravital microscopy. Adv Drug Deliv Rev 2006;58:770–772. [PubMed: 16971019]
10. Sidani M, Wyckoff J, Xue C, Segall JE, Condeelis J. Probing the microenvironment of mammary tumors using multiphoton microscopy. J Mammary Gland Biol Neoplasia 2006;11:151–163. 2006. [PubMed: 17106644]
11. Schluter K, Gassmann P, Enns A, et al. Organ-specific metastatic tumor cell adhesion and extravasation of colon carcinoma cells with different metastatic potential. Am J Pathol 2006;169:1064–1073. [PubMed: 16936278]
12. Naumov GN, Wilson SM, MacDonald IC, et al. Cellular expression of green fluorescent protein, coupled with high-resolution in vivo videomicroscopy, to monitor steps in tumor metastasis. J Cell Sci 1999;112(Pt 12):1835–1842. [PubMed: 10341203]
13. Martin MD, Fingleton B, Lynch CC, et al. Establishment and quantitative imaging of a 3D lung organotypic model of mammary tumor outgrowth. Clin Exp Metastasis 2008;25:877–885. [PubMed: 18787962]
14. Martin MD, Carter KJ, Jean-Philippe SR, et al. Effect of ablation or inhibition of stromal matrix metalloproteinase-9 on lung metastasis in a breast cancer model is dependent on genetic background. Cancer Research 2008;68:6251–6259. [PubMed: 18676849]
15. Gorden DL, Fingleton B, Crawford HC, Jansen DE, Lepage M, Matrisian LM. Resident stromal cell-derived MMP-9 promotes the growth of colorectal metastases in the liver microenvironment. Int J Cancer 2007;121:495–500. [PubMed: 17417772]
16. Weissman IL. Stem cells: units of development, units of regeneration, and units in evolution. Cell 2000;100:157–168. [PubMed: 10647940]
17. Coussens LM, Tinkle CL, Hanahan D, Werb Z. MMP-9 supplied by bone marrow-derived cells contributes to skin carcinogenesis. Cell 2000;103:481–490. [PubMed: 11081634]
18. Chantrain CF, Feron O, Marbaix E, Declerck YA. Bone marrow microenvironment and tumor progression. Cancer Microenviron 2008;1:23–35. [PubMed: 19308682]
19. Mendoza M, Khanna C. Revisiting the seed and soil in cancer metastasis. Int J Biochem Cell Biol 2009;41:1452–1462. [PubMed: 19401145]
20. Psaila B, Kaplan RN, Port ER, Lyden D. Priming the ‘soil’ for breast cancer metastasis: the pre-metastatic niche. Breast Dis 2006;26:65–74. [PubMed: 17473366]
21. Mook OR, Van Marle J, Vreeling-Sindelarova H, Jonges R, Frederiks WM, Van Noorden CJ. Visualization of early events in tumor formation of eGFP-transfected rat colon cancer cells in liver. Hepatology 2003;38:295–304. [PubMed: 12883473]
22. Haier J, Korb T, Hotz B, Spiegel HU, Senninger N. An intravital model to monitor steps of metastatic tumor cell adhesion within the hepatic microcirculation. J Gastrointest Surg 2003;7:507–514. discussion 514-505. [PubMed: 12763408]
23. Reichen J. The role of the sinusoidal endothelium in liver function. News Physio Sci 1999;14:117–121.
24. Qian B, Deng Y, Im JH, et al. A distinct macrophage population mediates metastatic breast cancer cell extravasation, establishment, and growth. PLoS ONE 2009;4:e6562. [PubMed: 19668347]
25. Carmeliet P, Jain RK. Angiogenesis in cancer and other diseases. Nature 2000;407:249–257. [PubMed: 11001068]
26. Fukumura D, Jain RK. Tumor microvasculature and microenvironment: targets for anti-angiogenesis and normalization. Microvasc Res 2007;74:72–84. [PubMed: 17560615]
27. Fukumura D, Jain RK. Imaging angiogenesis and the microenvironment. Apmis 2008;116:695–715. [PubMed: 18834413]

NIH-PA Author Manuscript

NIH-PA Author Manuscript

NIH-PA Author Manuscript

28. Inai T, Mancuso M, Hashizume H, et al. Inhibition of vascular endothelial growth factor (VEGF) signaling in cancer causes loss of endothelial fenestrations, regression of tumor vessels, and appearance of basement membrane ghosts. Am J Pathol 2004;165:35–52. [PubMed: 15215160]

29. Naumov GN, Akslen LA, Folkman J. Role of angiogenesis in human tumor dormancy: animal models of the angiogenic switch. Cell Cycle 2006:1779–87. [PubMed: 16931911]

NIH-PA Author Manuscript
NIH-PA Author Manuscript
NIH-PA Author Manuscript

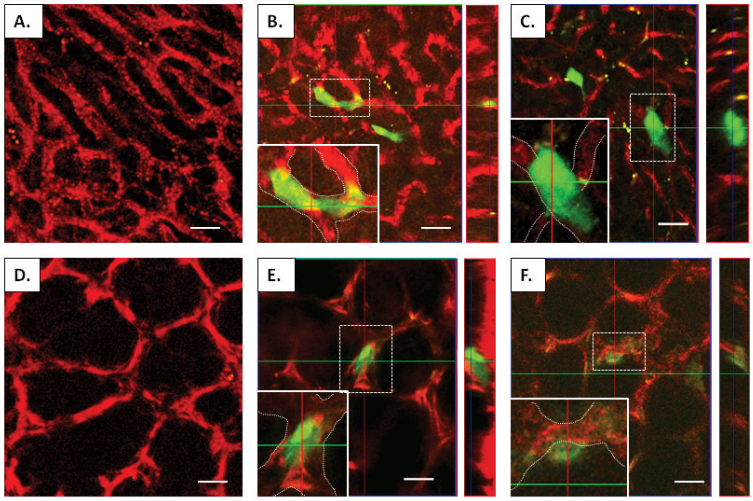

Figure 1.

Influence of the metastatic site on time to tumor cell extravasation. Micrographs of liver (A) and lung (D) whole organ preparations showing vasculature labeled with a tomato lectin-Qdot585 complex (red). Panels B and E show two-dimensional images and orthogonal images of a cell (in cross-hatch) either in the vasculature of the liver or the lung, respectively. *Inset of B and E*, magnified views of cells with vascular boundaries denoted by white dashes, showing the cells are completely within the confines of the liver or lung vasculature, respectively. Panels C and F denote both two-dimensional and orthogonal images of cells (in cross-hatch) that are outside the vasculature of the liver (C), or are in the process of extravasating from the vasculature of the lung (F). *Inset of C and F*, magnified views of cells with vascular boundaries denoted by white dashes. Note that in C and F the boundaries of the tumor cell extends beyond the delineated vascular boundaries, in contrast to panels B and E. Scale bar in all images= 25μm. The yellow debris present in panels B and C represents deposits of either lipid or vitamin A, which both have been shown previously to be autofluorescent in the liver.

NIH-PA Author Manuscript

NIH-PA Author Manuscript

NIH-PA Author Manuscript

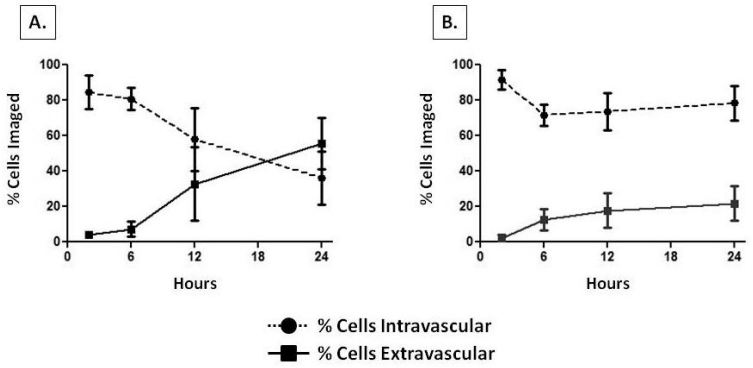

Figure 2.

Determination of time course of cellular extravasation in early breast cancer metastasis to liver and lung. Shown are graphical representations of the location of the percentage of cells imaged over the time course of the experiment in the liver (A) and the lung (B). Note that as the time point from injection to imaging gets longer, the percentage of cells that are extravascular increases in the liver, but does not change appreciably in the lung. Circles or squares represent the mean %, and error bars denote standard error.

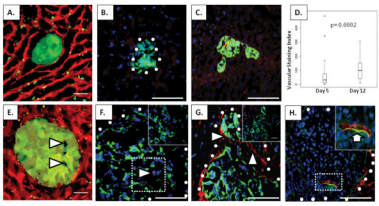

Figure 3.

Analysis of micrometastatic lesions in the liver. (A, E) Two-photon micrographs of R221A-GFP tumor foci (green) in the liver at 5 days (A) and 12 days (E) after tumor cell injection. A tomato lectin-Qdot585 complex was used to label the vasculature (red). *Arrowheads in E*, non-GFP labeled cells within the tumor foci. (B, F) Immunohistochemical staining for CD45 (red) in livers containing R221A-GFP tumors (green) at 5 days (B) and 12 days (F) after tumor cell injection. *Arrowhead in F*, cell stained positively for CD45. *Inset of outlined portion of F*, negative control for CD45. White circles denote the tumor/stroma boundaries. (C,G) Immunohistochemical staining for vWF (red) in livers containing R221A-GFP tumors (green) at 5 (C) and 12 (G) days following injection of tumor cells. Note the significant vWF positivity in endothelial cells throughout the tumor foci in (G) *(arrowheads)*. *Inset of (G)*, negative control for vWF. (D) Box plot of the vascular staining index based on vWF positivity in tumors of 5 day (42 tumors from 3 mice) and 12 day (44 tumors from 3 mice) lesions. The plots show the median, the 0.25, and the 0.75 quartiles of the data. Outliers are indicated as circles. (H) Immunohistochemical staining for vWF (green) with the Alexa Fluor 568 lectin/streptavadin conjugate (red) marking patent vessels at the 12 day time point. *Inset of (H)*, enlargement of outlined area with arrow indicating co-staining of vWF and Alexa Fluor in a patent vessel within the tumor foci. White circles denote the tumor/stroma boundaries. Cell nuclei (blue) were marked using Hoechst in panels B, C, F, G, and H. Scale bars on A, E= 25μm. Scale bars in B, C, F, G, and H= 50μm.

NIH-PA Author Manuscript NIH-PA Author Manuscript NIH-PA Author Manuscript

NIH-PA Author Manuscript

NIH-PA Author Manuscript

NIH-PA Author Manuscript

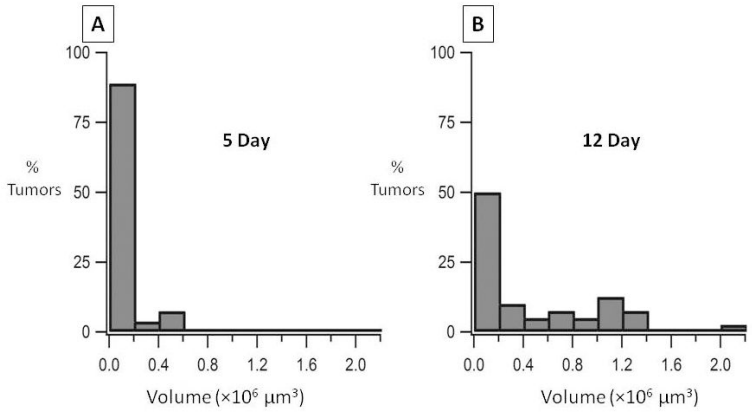

Figure 4.

Distribution of micrometastatic tumor volumes. A graphical representation of the distribution of tumor volumes is shown for imaged micrometastatic lesions using two photon microscopy at 5 days (N=27) (A) and 12 days (N=40) (B) after injection of R221A-GFP tumor cells. Representative images of 5 day and 12 day lesions are shown in Figure 3A and 3E.

NIH-PA Author Manuscript
NIH-PA Author Manuscript
NIH-PA Author Manuscript

Timepoint	Total # Cells Imaged	Total # Cells Intravascular (Mean % Cells Intravascular)	Total # Cells Extravascular (Mean % Cells Extravascular)	Total # of Uninformative Cells	Estimated Probability of Cells Being Extravascular	95% Confidence Interval
Liver Time Course						
2 Hour (n=2)	52	45 (85%)	2 (4%)	5	0.04	0.0065-0.1140
6 Hour (n=3)	90	72 (81%)	6 (7%)	12	0.07	0.0270-0.1305
12 Hour (n=3)	63	38 (58%)	19 (33%)	6	0.31	0.2012-0.4274
24 Hour (n=5)	146	54 (33%)	77 (56%)	15	0.5274*	0.4465-0.6074
Lung Time Course						
2 Hour (n=4)	42	37 (92%)	1 (2%)	4	0.02	0.0014-0.1006
6 Hour (n=4)	56	40 (72%)	7 (13%)	9	0.13	0.0557-0.2277
12 Hour (n=5)	59	41 (74%)	13 (18%)	5	0.22	0.1278-0.3366
24 Hour (n=3)	39	26 (78%)	5 (22%)	8	0.1282*	0.0480-0.2556

*P= 0.0001